Amphibian mast cells: barriers to deadly chytrid fungus infections

Authors: Kelsey A. Hauser[1], Muhammad R. H. Hossainey[1], Lindsey K. Gentry[2], Christina N. Garvey[1], Netra Ranganathan[1], Amulya Yaparla[1], Namarta Kalia[1], Mira Zelle[1], Elizabeth J. Jones[3], Anju N. Duttargi[3], Louise A. Rollins-Smith[4,5], Carly R. Muletz-Wolz[2], Leon Grayfer[1]*.

Affiliations:
[1]Department of Biological Sciences, The George Washington University, Washington, DC, USA.

[2]Center for Conservation Genomics, Smithsonian National Zoo & Conservation Biology Institute, Washington, DC, USA.

[3]Department of Oncology, Lombardi Comprehensive Cancer Center, Georgetown University, Washington DC, USA.

[4]Departments of Pathology, Microbiology and Immunology, and of Pediatrics, Vanderbilt University School of Medicine, Nashville, TN, USA.

[5]Department of Biological Sciences, Vanderbilt University, Nashville, TN, USA

*Corresponding author:
Suite 6000, 800 22nd St NW, Washington, DC 20052, USA.
Phone: 202-994-8076
Email: leon_grayfer@gwu.edu.

Keywords: mast cells, chytrid fungus, amphibian immunity, skin immunity

Abstract: Global amphibian declines are largely driven by deadly disease outbreaks caused by the chytrid fungus, *Batrachochytrium dendrobatidis* (*Bd*). In the time since these disease outbreaks were first discovered, much has been learned about the roles of amphibian skin-produced antimicrobial components and skin microbiomes in controlling *Bd*. Yet almost nothing is known about the roles of skin-resident immune cells in anti-*Bd* defenses. Notably, mammalian mast cells reside within and serve as key immune sentinels in barrier tissues like the skin. Thus, they are critical to immune recognition of pathogens and to orchestrating the ensuing immune responses. Accordingly, we investigated the roles of *Xenopus laevis* frog mast cells during *Bd* infections. Our findings indicate that enrichment of *X. laevis* skin mast cells confers significant anti-*Bd* protection and ameliorates the inflammation-associated skin damage caused by *Bd* infection. Moreover, enriching *X. laevis* mast cells promotes greater mucin content within cutaneous mucus glands and protects frogs from *Bd*-mediated changes to their skin microbiomes. Together, this work underlines the importance of amphibian skin-resident immune cells in anti-*Bd* defenses and introduces a novel approach for investigating amphibian host-chytrid pathogen interactions.

INTRODUCTION

Catastrophic declines of hundreds of amphibian species across six continents have been causally linked to the chytrid fungi, *Batrachochytrium dendrobatidis* (*Bd*) and *Batrachochytrium salamandrivorans* (*Bsal*)[1, 2]. Motile *Bd* zoospores readily colonize keratinized skin of adult amphibians and keratinized mouthparts of tadpoles[3]. *Bd* skin infections culminate in chytridiomycosis, ultimately disrupting the function of this respiratory and barrier tissue[3, 4, 5]. Effectively combatting chytrid infections requires a holistic understanding of amphibian cutaneous immune defenses. Research efforts up to this point have focused on antifungal capacities of amphibian skin-produced antimicrobial peptides[6, 7]; commensal antifungal products[7, 8, 9]; antifungal properties of mucus[9], alkaloids[10], and lysozymes[11, 12] as well as the roles of antibodies[4, 13]. Many of these studies suggest that *Bd* exposure can elicit some immune protection[14]. However, the contribution of skin-resident immune cells to amphibian anti-*Bd* defenses remains almost entirely unexplored.

Mammalian mast cells serve as sentinels of mucosal and connective tissues, concentrated in barrier tissues like skin, where they maintain homeostasis and regulate immune responses[15]. Other granulocyte-lineage cells such as neutrophils are generally not found in healthy tissues and only extravasate into sites of inflammation[16]. Consequently, mast cells are among the first immune cells to recognize and respond to skin-infiltrating pathogens. When activated, mast cells release pre-formed and *de novo*-generated immunomodulatory compounds that may serve to elicit, exacerbate, or ameliorate inflammatory responses[15]. Cells bearing hallmark mast cell cytology have been reported across a range of non-mammalian species[17, 18], including amphibians[19]. Notably, the principal mast cell growth factor, stem cell factor (SCF, KIT ligand) required for mast cell differentiation and survival[20] is expressed by all vertebrates examined to-date.

Here, we combine comprehensive *in vitro* and *in vivo* approaches to define the roles of amphibian (*Xenopus laevis*) mast cells during *Bd* infections. Our results provide compelling evidence that skin-resident immune cells contribute to anti-*Bd* defenses.

RESULTS

Frog mast cells possess archetypal mast cell cytology and transcriptional profiles

We produced *X. laevis* recombinant (r)SCF, and used this reagent to generate mast cell cultures from bone marrow-derived myeloid precursors[21]. Mast cells were compared to bone marrow-

derived neutrophilic granulocytes (hereafter referred to as 'neutrophils'), differentiated using a recombinant *X. laevis* colony-stimulating factor-3[21] (rCSF3, *i.e.*, granulocyte colony-stimulating factor; GCSF). While the neutrophil cultures were comprised of cells with hyper-segmented nuclei and neutral-staining cytoplasms (Fig. 1A), the mast cell cultures consisted predominantly of mononuclear cells with basophilic cytoplasm (Fig. 1B). We confirmed the granulocyte-lineage of *X. laevis* mast cells using specific esterase (SE) staining (Fig. 1D). As expected, *X. laevis* neutrophils were also SE-positive (Fig. 1C). Mast cell and neutrophil morphology was further explored with electron microscopy (Fig. 1E-H). SEM imaging demonstrated that *X. laevis* mast cells possess extensive folding of their plasma membranes (Fig. 1F). This mast cell-characteristic membrane ruffling appeared as projections resembling pseudopods via TEM, which further revealed electron-dense heterogenous granules, few mitochondria, and round to elongated nuclei (Fig. 1H) typical of mammalian mast cells[22]. *X. laevis* neutrophils also exhibited pronounced membrane ruffling (Fig. 1E) but strikingly distinct intracellular appearance including multilobed nuclei (Fig. 1G).

Frog mast cells and neutrophils also exhibited distinct transcriptional profiles of immune-related genes including those encoding lineage-specific transcription factors, immune receptors, downstream signaling components and adhesion molecules, as well as non-immune genes (Fig. 1I). Frog mast cells and neutrophils each expressed greater levels of lineage-specific transcription factors associated with mammalian mast cell (gata1, gata2, and mitf)[23] and neutrophil (cebp family members)[24] counterparts, respectively (Fig. 2A). Notably, mast cells expressed greater levels of enzyme and cytokine genes associated with tissue remodeling (carboxypeptidase; cpa[25]), immune suppression (indoleamine 2,3 dioxygenase-1; ido1[26]) and amelioration of cutaneous inflammation (leukemia inhibitory factor, lif[27]; Fig. 2B). Conversely, neutrophils expressed predominantly proinflammatory enzymes and cytokine genes such as leukotriene 4 hydrolase (lta4h; Fig. 2B) and tumor necrosis factor alpha (tnfα, Fig. 2B). In addition, mast cells and neutrophils each had greater expression of genes encoding their respective growth factor receptors, kit and csf3r (Fig. 2B).

Enriching mast cells in frog skin offers protection against *Bd*

Although all granulocyte-lineage cells possess SE activity, mast cells are the predominant mononuclear granulocytes to reside in vertebrate tissues[28]. Therefore, we selectively enriched mast cells in *X. laevis* skin via subcutaneous rSCF administration (note SE-stained cells indicated by

arrows in r-ctrl-injected skins, Fig. 3A, versus r-SCF-injected skins, Fig 3B). We confirmed SE-positive cells in rSCF-treated skins also possessed round-oval nuclei (Fig. 3C). Maximum mast cell enrichment was observed 12 hours post injection (hpi) of rSCF (Fig. 3D). When we challenged *X. laevis* with *Bd*, we did not detect differences in skin fungal loads between control (r-ctrl-injected) and mast cell-enriched groups at 7 days post infection (dpi; Fig. 3E). However, fungal loads were almost two-fold lower in mast cell- compared to control-enriched animals at 21 dpi, allowing for approximately four cycles of zoospore to mature zoosporangia development (Fig. 3E).

Mast cells protect frogs from *Bd*-elicited inflammation-associated pathology

To explore potential mechanisms of mast cell-mediated protection against *Bd,* we compared the gene expression profiles of r-ctrl- and rSCF-administered *Bd*-infected frog skins at 21 dpi. Among the top differentially expressed genes, we noted mast cell-enriched, *Bd*-infected skins possessed greater transcripts for genes associated with cutaneous strength and integrity (lamc2), epidermal cell maturation, lymphocyte recruitment (b3gnt3.1)[29, 30, 31], as well as ion and nutrient flow (gjb3l). (Fig. 4A). Moreover, mast cell-enriched *Bd*-challenged skin exhibited greater expression of genes associated with protection of the mucosa and epithelial healing (ttf3.6s)[32], pathogen nutrient deprivation in mucus (slc1a5s)[33], and mucus production (duoxa1.s[34]; Fig. 4A). In striking contrast, skins from control *Bd*-infected frogs revealed greater expression of genes associated with leukocyte infiltration and inflammation (*e.g.*, ccl19, cxcl16, adamt13, csf3r; Fig. 4A). These transcriptional profiles were supported by our histological observations wherein control *Bd*-infected skins exhibited hyperkeratosis, epidermal hyperplasia, jagged stratum corneum, and extensive leukocyte infiltration (Fig. 4B), while mast cell-enriched *Bd*-infected tissues appeared largely devoid of these pathologies (Fig. 4C).

Cutaneous neutrophil enrichment results in increased *Bd* fungal loads

Neutrophils are one of the first leukocytes to infiltrate infected tissues, typically amplifying inflammation[35]. All vertebrate neutrophils depend on CSF3 for their differentiation and function[36], and our previous work has demonstrated the gene encoding the CSF3 receptor (csf3r) is a marker of *X. laevis* neutrophils[37, 38]. Because csf3r expression was markedly elevated in control over mast cell-enriched skins of infected frogs (Fig. 4A), we next assessed the outcomes of enriching skin

for neutrophils via subcutaneous rCSF3 administration. We confirmed neutrophil enrichment peaked 12 hp rCSF3 injection (Fig. 4F) and resulted in a thickened epidermis in comparison with r-ctrl injected skins of otherwise healthy animals (*i.e.*, no *Bd*; Fig. 4D, E). When challenged with *Bd*, frogs with neutrophil-enriched skin possessed significantly greater *Bd* loads than control frogs (Fig. 4G). This suggests inflammation may be exacerbating *Bd* infections.

In vitro analyses of frog mast cells responses to *Bd*

Amphibians rely heavily on skin-produced antimicrobial peptides (AMPs) for antifungal protection[39], and mast cells produce antimicrobial AMPs[40]. Thus, we examined whether mast cells could be sources of such AMPs during *Bd* infections. As anticipated, mast cells, but not neutrophils challenged with *Bd*, upregulated their expression of the AMP-encoding genes, *pgla* and *magainin* (Fig. S1A).

Mammalian mast cells are recognized as potent producers of the pleotropic anti-inflammatory cytokine, interleukin-4 (IL4)[41]. Notably, *X. laevis* mast cells challenged *in vitro* with *Bd* significantly upregulated their il4 gene expression (Fig. S1A), whereas almost no il4 expression was detected from either unstimulated or *Bd*-challenged neutrophils. To examine whether the frog IL4 might offer anti-*Bd* protection, we generated the *X. laevis* IL4 in recombinant form (rIL4) and confirmed subcutaneous injection of this moiety augmented expression of genes typically activated by the mammalian IL4[42] (cd36, metalloproteinase inhibitor 3-timp3, and monoamine oxidase A-maoa; Fig. S1B). However, subcutaneous administration of rIL4 in *Bd*-infected frogs did not alter their fungal loads (Fig. S1C), suggesting IL4 is probably not a major mechanism responsible for the observed mast cell-mediated anti-*Bd* protection.

Enrichment of frog skin mast cells alters mucus gland composition

Because mast cell-enriched frog skin had greater expression of genes associated with mucosal tissue integrity and mucus production (Fig. 4A), we next investigated whether the anti-*Bd* protection identified in mast cell-enriched skins could be due, at least in part, to differences in mucus production. Interestingly, while mucus glands in mock- and *Bd*-infected control skin sections contained normal levels of mucus, those from both mock- and *Bd*-infected frogs that had been enriched for cutaneous mast cells were significantly more filled with higher levels of mucin (Fig. 5A-C).

Enrichment of frog skin mast cells alters skin microbial composition

Amphibian skin-produced mucus may offer antimicrobial protection and serve as a selective substratum for commensal microbes, many of which are antifungal[9]. We found no significant differences in direct *Bd*-killing capacities of mucus isolated from mock- or *Bd*-challenged control or mast cell-enriched frogs (Fig. S2). By contrast, we observed substantial differences in skin microbiomes, including changes in bacterial composition and richness as well as relative abundances of *Bd*-inhibitory bacteria (Fig. 5D-G, Fig. S3). A total of 1645 bacterial amplicon sequence variants (ASVs) were identified from 20 bacterial phyla, seven of which were predominant (Fig. 5D). Of these, *Verrucomicrobiota* were only present on uninfected animals, whereas *Acidobacteriota* was only seen after 21 dpi on both control and mast cell-enriched, infected animals (Fig. 5D).

At 10 dpi, mast cell-enrichment resulted in a nominal shift in community composition compared to control frogs (Fig. 5E). Notably, while control, *Bd*-infected animals exhibited a drastic shift in community composition, mast cell-enriched animals possessed substantially less deviated community composition (Fig. 5E), suggesting that these cells are somehow counteracting the adverse effects of *Bd* on microbiome structure. These mast cell-mediated effects persisted to 21 dpi (Fig. S3A).

At 10 dpi, mast cell-enriched and mock-infected frogs possessed significantly greater abundance of *Bd*-inhibitory bacteria such as *Chyrseobacterium sp*., compared to control, mock infected animals (Fig. 5F)[43]. This suggests that mast cells may promote skin flora composition that is more antifungal. Control (non-enriched) *Bd*-infected frogs possessed significantly greater abundance of *Bd*-inhibitory bacteria than all other treatment groups (Fig. 5F). While mast cell-enriched, *Bd*-infected frogs had lower abundance of *Bd*-inhibitory bacteria than control infected frogs, they possessed higher abundance of inhibitory taxa than uninfected control animals (Fig. 5F). The *Bd*-inhibitory bacteria seen in greater abundance on mast cell-enriched, *Bd*-infected animals, included *Roseateles sp*., *Flavobacterium sp.*, and *Kaistia sp*. We did not see significant differences in *Bd*-inhibitory bacteria across the treatment groups at 21 dpi (Fig. S3B).

Mast cell-enriched uninfected frogs exhibited increased frog skin bacterial richness at 10 dpi (Fig. 5G). While control *Bd*-infected animals exhibited significantly reduced skin microbial richness, mast cell-enriched *Bd*-infected frogs did not exhibit such a reduction in bacterial richness

(Fig. 5G), supporting the idea that mast cells may be counteracting the adverse effects of *Bd* on skin microbiome composition.

DISCUSSION

Amphibian extinction rates far outpace those of any other vertebrate class[44]. It is now well-established that chytrid fungi are major contributors to these declines, and strikingly, are considered the greatest infectious disease threat to biodivsersity[45]. The development of effective mitigation strategies though, is hindered by incomplete understanding of amphibian immune defenses and skin integrity. In this respect, while mast cells are recognized as key immune sentinels of tissues such as skin[46], relatively little is known about this cell lineage outside of mammals. Our findings provide the first in-depth functional analyses of these cells in amphibians and explore their protective mechanisms during chytrid infections. This work presents a unique perspective on the evolution of mast cell functionality and will serve as a new avenue to explore ways to counteract the amphibian declines.

Mammalian mast cells directly interact with neurons innervating the skin[47], and mucus production in mammals is tightly controlled by neuronal signaling[48]. In turn, mucus serves as a critical substratum for microbiota at mucosal barriers[49]. Here, we demonstrate that frog skin mast cells appear to confer significant protection against *Bd* by counteracting *Bd*-elicited inflammation, maintaining skin integrity, promoting mucus production, and preventing the disassembly of established skin microbiomes. Amphibian skin is much thinner and more permeable than that of mammals[7], and as such, arguably represents a more penetrable barrier to pathogens. Because mammalian skin is relatively impermeable, mast cells are absent from mammalian epidermis and are instead found exclusively in their dermal layers[50]. In contrast, we have shown here and have observed across several classes of amphibians[16] that mast cells are found in both epidermal and dermal layers. This localization has presumably evolved to support the more intimate contact between amphibian skin and their environments. Considering the importance of amphibian cutaneous integrity to their physiology[51], it is likely that skin-resident mast cells co-evolved to support skin immunity, physiology, and symbiotic microbiota. Ongoing research continues to reveal functional differences between mammalian connective tissue and mucosa-resident mast cells[52], and we suspect that there is similarly much to learn about the distinct physiological and immune roles of amphibian epidermal and dermal mast cells.

Bd infections caused major reductions in bacterial taxa richness, changes in composition and substantial increases in the relative abundance of *Bd*-inhibitory bacteria early in the infection. Similar changes to microbiome structure occur during experimental *Bd* infections of red-backed salamanders and mountain yellow-legged frogs[8, 53]. In turn, progressing *Bd* infections corresponded with a return to baseline levels of *Bd*-inhibitory bacteria abundance and rebounding microbial richness, albeit with dissimilar communities to those seen in control animals. These temporal changes indicate that amphibian microbiomes are dynamic, as are the effects of *Bd* infections on them. Indeed, *Bd* infections may have long-lasting impacts on amphibian microbiomes[8]. While *Bd* infections manifested in these considerable changes to frog skin microbiome structure, mast cell enrichment appeared to counteract these deleterious effects to their microbial composition. Presumably, the greater skin mucosal integrity and mucus production observed after mast cell enrichment served to stabilize the cutaneous environment during *Bd* infections, thereby ameliorating the *Bd*-mediated microbiome changes. While this work explored the changes in established antifungal flora, we anticipate the mast cell-mediated inhibition of *Bd* may be due to additional, yet unidentified bacterial or fungal taxa. Intriguingly, while mammalian skin mast cell functionality depends on microbiome elicited SCF production by keratinocytes[54], our results indicate that frog skin mast cells in turn impact skin microbiome structure and likely their function. It will be interesting to further explore the interdependent nature of amphibian skin microbiomes and resident mast cells.

In contract to the mast cell effects, enrichment of neutrophils seemed to result in greater *Bd* skin burdens. This suggests that neutrophils and the cytokines they release may result in a greater level of inflammation, which is not protective. This is consistent with other studies that suggest that a strong immune response in the skin compartment of some species may be detrimental[55, 56]

It has become apparent that amphibian host-*Bd* interactions are highly complex and multifaceted while different amphibian species exhibit marked differences in their susceptibilities to this devastating pathogen[2, 4]. The findings described here emphasize the importance of skin-resident mast cells for successful anti-*Bd* defenses and demonstrate that these immune sentinels are intimately linked to many aspects of frog skin physiology. Our results indicate that when mast cells are enriched, the ensuing changes in the skin allow for greater resistance to infection by developing zoospores. Presumably, distinct amphibian species have evolved disparate

interconnections between their skin mast cells and their cutaneous defenses, as dictated by their respective physiological and environmental pressures. In turn, these species-specific differences likely dictate whether and to what extent the skin-resident mast cells of a given amphibian species recognize and appropriately respond to *Bd* infections. We postulate that such differences may contribute to the differences in susceptibilities of amphibian species to pathogens like chytrid fungi.

METHODS

Animals

Outbred 1 year-old (1.5-2"), mixed sex *X. laevis* were purchased from Xenopus 1 (Dexter, MI). All animals were housed and handled under strict laboratory regulations as per GWU IACUC (Approval number 15-024).

Recombinant cytokines and bone marrow granulocyte cultures

The *X. laevis* rSCF, rCSF3 and rIL4 were generated as previously described for rCSF3[57] and as detailed in the supplemental materials.

Bone marrow isolation, culture conditions, and establishment of neutrophil cultures have been previously described[58]. Mast cell cultures were generated according to protocols adapted from Koubourli et al. (2018) and Meurer et al. (2016) [59, 60]. Isolated bone marrow cells were treated with 250 ng/µl of rSCF on Day 0, Day 4, Day 7, and collected for further analysis on Day 9. Cell cultures were maintained at 27°C with 5% CO_2 in amphibian medium supplemented with 10% fetal bovine serum and 0.25% *X. laevis* serum. Neutrophil-like granulocytes were generated as above but with 250 ng/µl of rCSF3 on Day 0, Day 3, and collected for further analysis on Day 5. Cell cultures were maintained at 27°C with 5% CO_2 in amphibian serum-free medium supplemented with 10% fetal bovine serum, 0.25% *X. laevis* serum, 10 µg/mL gentamicin (Thermo Fisher Scientific, Waltham, Massachusetts, USA), 100 U/mL penicillin, and 100 µg/mL streptomycin (Gibco, Thermo Fisher Scientific).

Enrichment of skin granulocyte subsets

Animals were subcutaneously injected between the skin and muscle layers with 5 µg/animal of rSCF, rCSF3, or r-ctrl in 5 µL of saline using finely pulled glass needles. Optimal time course and

dose for *in vivo* mast cell and neutrophil enrichment were determined during preliminary experiments.

Recombinant interleukin-4 treatment

The capacity of the recombinant interleukin-4 (rIL4) to induce expression of genes associated with mammalian IL4 responses were assessed by injecting frogs (*N*=6 per treatment group subcutaneously with rIL4 (5 µg/animal) or r-ctrl in 5 µl of saline. After 6hrs, animals were sacrificed, and skins were isolated for gene expression analyses.

To examine the effect of rIL4 on *Bd* loads, frogs were infected with *Bd* by water bath (10^5 zoospores/mL) as described below and 1 day later injected subcutaneously, dorsally with rIL4 (5 µg/animal) or r-ctrl in 5 µl of saline. After an additional 9 days of infection, animals were sacrificed and their dorsal skin *Bd* loads examined.

***Bd* stocks and fungal challenge**

Bd isolate JEL 197 was grown in 1% tryptone broth or on 1% tryptone agar plates (Difco Laboratories, Detroit, MI) supplemented with 100 U/mL penicillin and 100 µg/mL streptomycin (Gibco) at 19°C.

In vitro Bd killing was evaluated by incubating live *Bd* (maturing zoosporangia) with mast cells or neutrophils at ratios of 5:1 or 1:1 *Bd* cells per granulocyte. Cells were incubated at 27°C for three days before fungal loads were analyzed by absolute qPCR. Experimental groups were compared to pathogen DNA amounts derived from equal quantities of live *Bd* plated alone in otherwise identical conditions.

For *in vivo* infection studies, zoospores were harvested by flooding confluent tryptone agar plates with 2 mL sterile A-PBS for 10 minutes. Twelve hours post rSCF, rCSF3, rIL4, or r-ctrl injection, animals were infected with 10^7 zoospores or mock-infected in 100 mL of water (10^5 zoospores/mL). After 3 hrs, 400 mL of water was added to each tank. Skins were collected for histology and gene expression analysis on 1, 7, and 21 dpi.

Histology

X. laevis leukocyte cytology and cutaneous SE staining has been described[57] and is detailed in the supplemental materials. An Alcian Blue/PAS staining kit (Newcomer Supply, Middleton, WI) was

used to quantify mucin content from *in vivo* experiments. Histological analyses are detailed in the supplemental materials.

Electron Microscopy

Processing and imaging of cells for transmission and scanning electron microscopy (TEM and SEM) was conducted at the GWU Nanofabrication and Imaging Center (GWNIC). For transmission electron microscopy, cells were fixed as monolayers on six-well plates with 2.5% glutaraldehyde and 1% paraformaldehyde in 0.1 M sodium cacodylate buffer for one hour. Cells were treated with 1% osmium tetroxide in 0.1 M sodium cacodylate buffer for 1 hr. Following washes, cells were *en bloc* stained with 1% uranyl acetate in water overnight at 4°C. Samples were dehydrated through an ethanol series and embedded in epoxy resin using LX112. Inverted Beem capsules were placed into each tissue culture well to create *on face* blockfaces for sectioning. Resin was cured for 48 hrs at 60°C. The 95 nm sections were post-stained with 1% aqueous uranyl acetate and Reynold's lead citrate. All imaging was performed at 80 KV in a Talos 200X transmission electron microscope (Thermo Fisher Scientific, Hillsboro, OR).

For SEM, cells were fixed with 2.5% glutaraldehyde / 1% paraformaldehyde in Sodium cacodylate buffer, followed by 1% OsO_4, then dehydrated through an ethyl alcohol series. Coverslips were critical point dried and coated with 2 nm iridium. Cells were imaged using a Teneo Scanning Electron Microscope (Thermo Fisher Scientific).

Analyses of immune gene expression and *Bd* skin loads

These analyses have been described[57] and are detailed in supplemental materials.

RNA sequencing

For transcriptomic profiling, bone marrow-derived neutrophil and mast cell cultures were generated as described above and FACS-sorted according to preestablished size and internal complexity parameters to isolate the respective subsets for further analyses. Sorted cells were immediately processed to extract and purify RNA. Flash frozen samples were sent to Azenta Life Sciences for all library preparation, RNA sequencing, and analyses. In short, polyadenylated RNA was isolated using Oligo dT beads. Enriched mRNAs were then fragmented for first and second strand cDNA synthesis. cDNA fragments were end repaired, 5' phosphorylated, and dA-tailed.

Fragments were then ligated to universal adaptors and PCR-amplified. 150-bp paired-end sequencing was performed on an Illumina HiSeq platform.

FastQC was used to evaluate raw data quality. Adaptors sequences and poor-quality nucleotides were removed from reads using Trimmomatic v.0.36. The STAR aligner v.2.55.2b was used to map these reads to the Xenopus_laevis_9_2 reference genome from ENSEMBL. To determine differential gene expression, featureCount (Subread package v.1.5.2) was first used to count unique gene hits, which were then used with DESeq2 to calculate absolute $\log_2$-fold change.

Skin microbiome analyses

Towards microbiome studies, frogs were housed individually (N=6/treatment group). At indicated times, frogs were gently rinsed with sterile deionized water to remove transient microbes and gently swabbed 20 times, dorsally. Genomic DNA was extracted from swabs using a PowerSoil Pro kit on a Qiacube HT (QIAGEN, MD). One-step PCR library prep and dual-index paired-end Illumina sequencing was used to sequence the skin microbiome of individual frogs. A ~380 base pair region in the V3-V5 region of the 16S rRNA gene using the universal primers 515F-Y (GTGYCAGCMGCCGCGGTAA) and 939R (CTTGTGCGGGCCCCCGTCAATTC) was used for amplification. Negative and positive controls (ZymoBIOMICS D6300 & D6305, Zymo, CA) were included in each round of extraction and PCR. Reactions were done in duplicate for each sample, pooled, cleaned with in-house Speed-beads (in a PEG/NaCl buffer), quantified with a Qubit4 (Invitrogen, MA) and pooled into a final library in equimolar proportion. The pooled library was sequenced on two Illumina MiSeq runs (v3 chemistry: 2x300 bp kit) at the Center for Conservation Genomics, Smithsonian National Zoo & Conservation Biology Institute.

Analyses were performed in the R environment version 4.0.3 (R Core Team, 2020) using methods detailed in the supplemental materials.

Statistical analyses

Differences in transcript expression were calculated with one-way or multi-way ANOVAs followed by Tukey post-hoc tests. Student's t-tests were used to determine differences in *Bd* loads between treatments only. Statistical differences in mucin content and mucosome *Bd*-killing were assessed with the two-way ANOVA calculator available online through Statistics Kingdom. For

RNA sequencing, *p*-values were calculated with the Wald test and were adjusted using the Benjamini-Hochberge procedure.

ACKNOWLEDGMENTS:

We thank Dr. Cynthia S. Dowd and Ben England (Chemistry Department, GWU) for their help with *X. laevis* mucus lyophilization. We thank Dr. Christine Brantner (GWU Nanofabrication and imaging center) for assistance with TEM and SEM imaging. KAH, MRHH, and AY were supported by Wilbur V. Harlan summer graduate research fellowships. KAH, MRHH, NR, NK, AY, MZ, and LG thank the GWU Biology Department.

Funding:

National Science Foundation grant 2131061 (LG, CRMW)
National Science Foundation grant 2147466 (LG, LAR-S)
National Science Foundation grant 2147467 (LAR-S)

Author contributions:

Conceptualization: KAH, LG

Methodology: KAH, MRHH, LKG, CNG, NR, NK, AY, MZ, EJJ, AND, LAR-S, CRMW, LG

Investigation: KAH, MRHH, LKG, CNG, NR, NK, AY, MZ, EJJ, AND, LAR-S, CRMW, LG

Visualization: KAH, MRHH, EJJ, AND, LG

Funding acquisition: LG, CRMW, LAR-S

Project administration: LG

Supervision: LG, CRMW, LAR-S

Writing – original draft: KAH, LAR-S, CRMW, LG

Writing – review & editing: KAH, LAR-S, CRMW, LG

Competing interests: The authors declare no competing interests.

Data and materials availability: All data are available in the main text or the supplementary materials.

REFERENCES

1. Martel, A. *et al.* Wildlife disease. Recent introduction of a chytrid fungus endangers Western Palearctic salamanders. *Science* **346**, 630-631 (2014).

2. Scheele, B.C. *et al.* Amphibian fungal panzootic causes catastrophic and ongoing loss of biodiversity. *Science* **363**, 1459-1463 (2019).

3. Van Rooij, P., Martel, A., Haesebrouck, F. & Pasmans, F. Amphibian chytridiomycosis: a review with focus on fungus-host interactions. *Veterinary research* **46**, 1-22 (2015).

4. Van Rooij, P. *et al.* Development of in vitro models for a better understanding of the early pathogenesis of Batrachochytrium dendrobatidis infections in amphibians. *Altern Lab Anim* **38**, 519-528 (2010).

5. Voyles, J. *et al.* Pathogenesis of chytridiomycosis, a cause of catastrophic amphibian declines. *Science* **326**, 582-585 (2009).

6. Rollins-Smith, L.A. The importance of antimicrobial peptides (AMPs) in amphibian skin defense. *Dev Comp Immunol* **142**, 104657 (2023).

7. Varga, J.F.A., Bui-Marinos, M.P. & Katzenback, B.A. Frog Skin Innate Immune Defences: Sensing and Surviving Pathogens. *Front Immunol* **9**, 3128 (2018).

8. Jani, A.J. *et al.* The amphibian microbiome exhibits poor resilience following pathogen-induced disturbance. *ISME J* **15**, 1628-1640 (2021).

9. Woodhams, D.C., McCartney, J., Walke, J.B. & Whetstone, R. The adaptive microbiome hypothesis and immune interactions in amphibian mucus. *Dev Comp Immunol*, 104690 (2023).

10. Rodriguez, C., Rollins-Smith, L., Ibanez, R., Durant-Archibold, A.A. & Gutierrez, M. Toxins and pharmacologically active compounds from species of the family Bufonidae (Amphibia, Anura). *J Ethnopharmacol* **198**, 235-254 (2017).

11. Grogan, L.F. *et al.* Review of the Amphibian Immune Response to Chytridiomycosis, and Future Directions. *Front Immunol* **9**, 2536 (2018).

12. Rollins-Smith, L.A. *et al.* Immune defenses of Xenopus laevis against Batrachochytrium dendrobatidis. *Front Biosci (Schol Ed)* **1**, 68-91 (2009).

13. Ramsey, J.P., Reinert, L.K., Harper, L.K., Woodhams, D.C. & Rollins-Smith, L.A. Immune defenses against Batrachochytrium dendrobatidis, a fungus linked to global amphibian declines, in the South African clawed frog, Xenopus laevis. *Infect Immun* **78**, 3981-3992 (2010).

14. McMahon, T.A. *et al.* Amphibians acquire resistance to live and dead fungus overcoming fungal immunosuppression. *Nature* **511**, 224-227 (2014).

15. Sobiepanek, A. *et al.* The multifaceted roles of mast cells in immune homeostasis, infections and cancers. *International Journal of Molecular Sciences* **23**, 2249 (2022).

16. Hauser, K.A., Garvey, C.N., Popovic, M. & Grayfer, L. Biology of amphibian granulocytes - From evolutionary pressures to functional consequences. *Dev Comp Immunol* **140**, 104623 (2023).

17. McNeil, H.P., Adachi, R. & Stevens, R.L. Mast cell-restricted tryptases: structure and function in inflammation and pathogen defense. *Journal of Biological Chemistry* **282**, 20785-20789 (2007).

18. Abraham, S.N. & St John, A.L. Mast cell-orchestrated immunity to pathogens. *Nature reviews.Immunology* **10**, 440-452 (2010).

19. Baccari, G.C., Pinelli, C., Santillo, A., Minucci, S. & Rastogi, R.K. Mast cells in nonmammalian vertebrates: an overview. *International review of cell and molecular biology* **290**, 1-53 (2011).

20. Ito, T. *et al.* Stem cell factor programs the mast cell activation phenotype. *J Immunol* **188**, 5428-5437 (2012).

21. Yaparla, A., Wendel, E.S. & Grayfer, L. The unique myelopoiesis strategy of the amphibian Xenopus laevis. *Developmental & Comparative Immunology* **63**, 136-143 (2016).

22. Espinosa-Riquer, Z.P. *et al.* Signal transduction pathways activated by innate immunity in mast cells: translating sensing of changes into specific responses. *Cells* **9**, 2411 (2020).

23. Cildir, G. *et al.* Understanding mast cell heterogeneity at single cell resolution. *Trends in Immunology* **42**, 523-535 (2021).

24. Paudel, S., Ghimire, L., Jin, L., Jeansonne, D. & Jeyaseelan, S. Regulation of emergency granulopoiesis during infection. *Front Immunol* **13**, 961601 (2022).

25. Atiakshin, D. *et al.* Carboxypeptidase A3-A Key Component of the Protease Phenotype of Mast Cells. *Cells* **11** (2022).

26. Baban, B. *et al.* IDO activates regulatory T cells and blocks their conversion into Th17-like T cells. *J Immunol* **183**, 2475-2483 (2009).

27. Banner, L.R., Patterson, P.H., Allchorne, A., Poole, S. & Woolf, C.J. Leukemia inhibitory factor is an anti-inflammatory and analgesic cytokine. *J Neurosci* **18**, 5456-5462 (1998).

28. Agis, H. *et al.* Mast Cell-Lineage Versus Basophil Lineage Involvement in Myeloproliferative and Myelodysplastic Syndromes: Diagnostic Role of Cell-Immunopheno typing. *Leukemia & lymphoma* **22**, 187-204 (1996).

29. Kiritsi, D., Has, C. & Bruckner-Tuderman, L. Laminin 332 in junctional epidermolysis bullosa. *Cell adhesion & migration* **7**, 135-141 (2013).

30. Chang, E.H., Van Camp, G. & Smith, R.J. The role of connexins in human disease. *Ear and hearing* **24**, 314-323 (2003).

31. Pereira, M.S. *et al.* Glycans as key checkpoints of T cell activity and function. *Frontiers in immunology* **9**, 2754 (2018).

32. Taupin, D. & Podolsky, D.K. Trefoil factors: initiators of mucosal healing. *Nat Rev Mol Cell Biol* **4**, 721-732 (2003).

33. Kandasamy, P., Gyimesi, G., Kanai, Y. & Hediger, M.A. Amino acid transporters revisited: New views in health and disease. *Trends Biochem Sci* **43**, 752-789 (2018).

34. Fischer, H. Mechanisms and function of DUOX in epithelia of the lung. *Antioxid Redox Signal* **11**, 2453-2465 (2009).

35. Wang, J. Neutrophils in tissue injury and repair. *Cell Tissue Res* **371**, 531-539 (2018).

36. Roberts, A.W. G-CSF: a key regulator of neutrophil production, but that's not all! *Growth Factors* **23**, 33-41 (2005).

37. Koubourli, V.D., Wendel, E.S., Yaparla, A., Ghaul, J.R. & Grayfer, L. Immune roles of amphibian (Xenopus laevis) tadpole granulocytes during Frog Virus 3 ranavirus infections. *Dev Comp Immunol* **72**, 112-118 (2017).

38. Yaparla, A., Wendel, E.S. & Grayfer, L. The unique myelopoiesis strategy of the amphibian Xenopus laevis. *Dev Comp Immunol* **63**, 136-143 (2016).

39. Patocka, J., Nepovimova, E., Klimova, B., Wu, Q. & Kuca, K. Antimicrobial peptides: amphibian host defense peptides. *Current medicinal chemistry* **26**, 5924-5946 (2019).

40. Di Nardo, A., Yamasaki, K., Dorschner, R.A., Lai, Y. & Gallo, R.L. Mast cell cathelicidin antimicrobial peptide prevents invasive group A Streptococcus infection of the skin. *J Immunol* **180**, 7565-7573 (2008).

41. Babina, M., Guhl, S., Artuc, M. & Zuberbier, T. IL-4 and human skin mast cells revisited: reinforcement of a pro-allergic phenotype upon prolonged exposure. *Archives of dermatological research* **308**, 665-670 (2016).

42. Bhattacharjee, A. *et al.* IL-4 and IL-13 employ discrete signaling pathways for target gene expression in alternatively activated monocytes/macrophages. *Free Radic Biol Med* **54**, 1-16 (2013).

43. Woodhams, D.C. *et al.* Antifungal isolates database to centralize data on amphibian ski associated bacteria and their function against emerging fungal pathogens including Batrachochytrium dendrobatidis. *Ecology* **96**, 595 (2015).

44. https://www.iucnredlist.org/resources/summary-statistics, I.R.L.

45. Fisher, M.C. & Garner, T.W. Chytrid fungi and global amphibian declines. *Nature Reviews Microbiology* **18**, 332-343 (2020).

46. St. John, A.L., Rathore, A.P. & Ginhoux, F. New perspectives on the origins and heterogeneity of mast cells. *Nature Reviews Immunology* **23**, 55-68 (2023).

47. Zhang, S., Sumpter, T.L. & Kaplan, D.H. Neuron–Mast Cell Cross-Talk in the Skin. *J Invest Dermatol* **142**, 841-848 (2022).

48. Baraniuk, J.N. Neural regulation of mucosal function. *Pulm Pharmacol Ther* **21**, 442-448 (2008).

49. Paone, P. & Cani, P.D. Mucus barrier, mucins and gut microbiota: the expected slimy partners? *Gut* **69**, 2232-2243 (2020).

50. Cowen, T., Trigg, P. & Eady, R.A. Distribution of mast cells in human dermis: development of a mapping technique. *Br J Dermatol* **100**, 635-640 (1979).

51. Larsen, E.H. Dual skin functions in amphibian osmoregulation. *Comparative Biochemistry and Physiology Part A: Molecular & Integrative Physiology* **253**, 110869 (2021).

52. West, P.W. & Bulfone-Paus, S. Mast cell tissue heterogeneity and specificity of immune cell recruitment. *Front Immunol* **13**, 932090 (2022).

53. Muletz-Wolz, C.R., Fleischer, R.C. & Lips, K.R. Fungal disease and temperature alter skin microbiome structure in an experimental salamander system. *Mol Ecol* **28**, 2917-2931 (2019).

54. Wang, Z. *et al.* Skin microbiome promotes mast cell maturation by triggering stem cell factor production in keratinocytes. *J Allergy Clin Immunol* **139**, 1205-1216 e1206 (2017).

55. Ellison, A.R. *et al.* More than skin deep: functional genomic basis for resistance to amphibian chytridiomycosis. *Genome Biol Evol* **7**, 286-298 (2014).

56. Savage, A.E., Gratwicke, B., Hope, K., Bronikowski, E. & Fleischer, R.C. Sustained immune activation is associated with susceptibility to the amphibian chytrid fungus. *Mol Ecol* **29**, 2889-2903 (2020).

57. Hauser, K. *et al.* Discovery of granulocyte-lineage cells in the skin of the amphibian Xenopus laevis. *FACETS* **5**, 571 (2020).

58. Yaparla, A. & Grayfer, L. Isolation and culture of amphibian (Xenopus laevis) sub-capsular liver and bone marrow cells. *Xenopus: Methods and Protocols*, 275-281 (2018).

59. Koubourli, D.V., Yaparla, A., Popovic, M. & Grayfer, L. Amphibian (Xenopus laevis) interleukin-8 (CXCL8): a perspective on the evolutionary divergence of granulocyte chemotaxis. *Frontiers in immunology*, 2058 (2018).

60. Meurer, S.K. *et al.* Isolation of mature (peritoneum-derived) mast cells and immature (bone marrow-derived) mast cell precursors from mice. *PLoS One* **11**, e0158104 (2016).

61. Callahan, B.J. *et al.* DADA2: High-resolution sample inference from Illumina amplicon data. *Nat Methods* **13**, 581-583 (2016).

62. McMurdie, P.J. & Holmes, S. phyloseq: an R package for reproducible interactive analysis and graphics of microbiome census data. *PLoS One* **8**, e61217 (2013).

63. Davis, N.M., Proctor, D.M., Holmes, S.P., Relman, D.A. & Callahan, B.J. Simple statistical identification and removal of contaminant sequences in marker-gene and metagenomics data. *Microbiome* **6**, 226 (2018).

64. Jimenez, R.R. *et al.* Inhibitory Bacterial Diversity and Mucosome Function Differentiate Susceptibility of Appalachian Salamanders to Chytrid Fungal Infection. *Appl Environ Microbiol* **88**, e0181821 (2022).

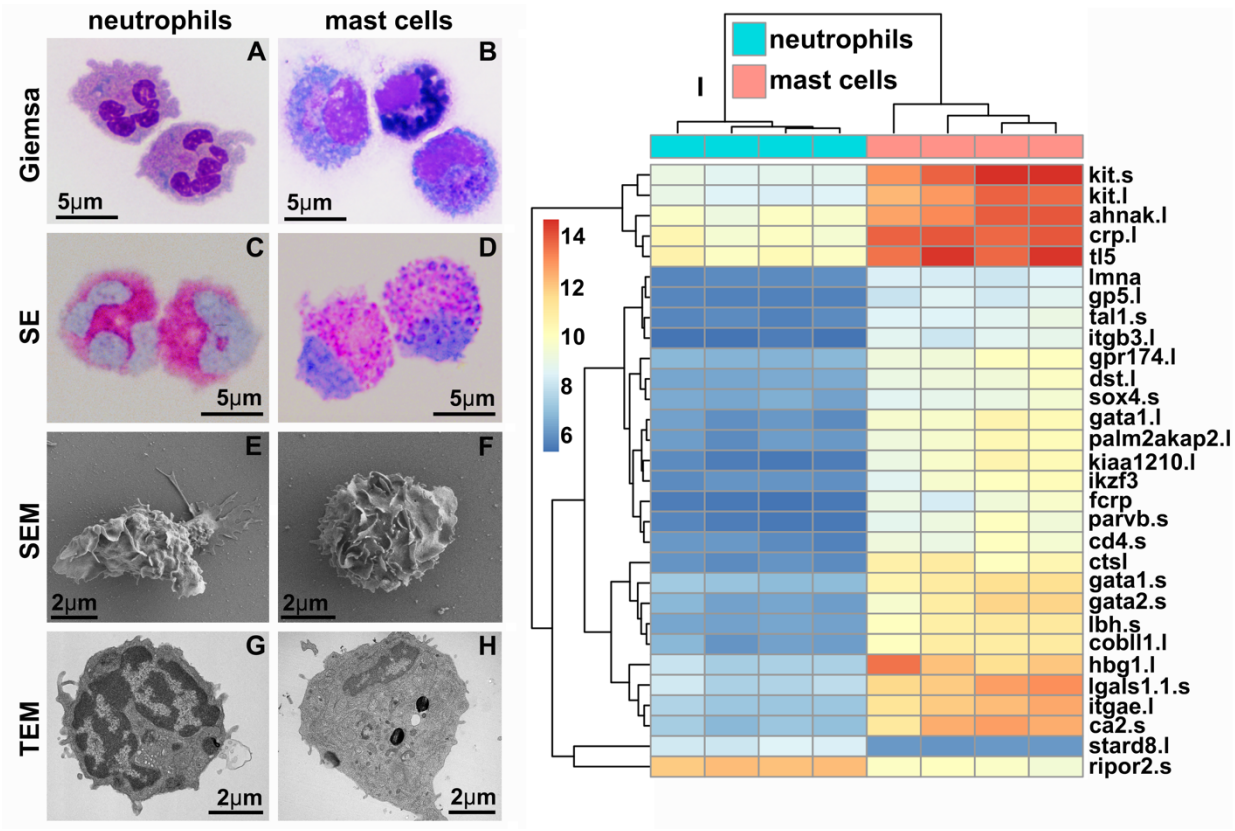

Figure 1. *X. laevis* bone marrow-derived mast cells possess classical mast cell cytology and transcriptional profiles. Neutrophils (**A**, **C**, **E**, **G**) and mast cells (**B**, **D**, **F**, **H**) were stained with Giemsa (**A**, **B**) and Leder to visualize specific esterase activity (SE) (**C**, **D**) or imaged with scanning and transmission electron microscopy (SEM: **E**, **F** and TEM: **G**, **H**). (**I**) Heat map of the top 30 differentially expressed genes (DEGs) identified with RNA sequencing analyses of *X. laevis* mast cell (*N*=4) and neutrophil (*N*=4) cultures. Log_2fold change in expression represented as color scale.

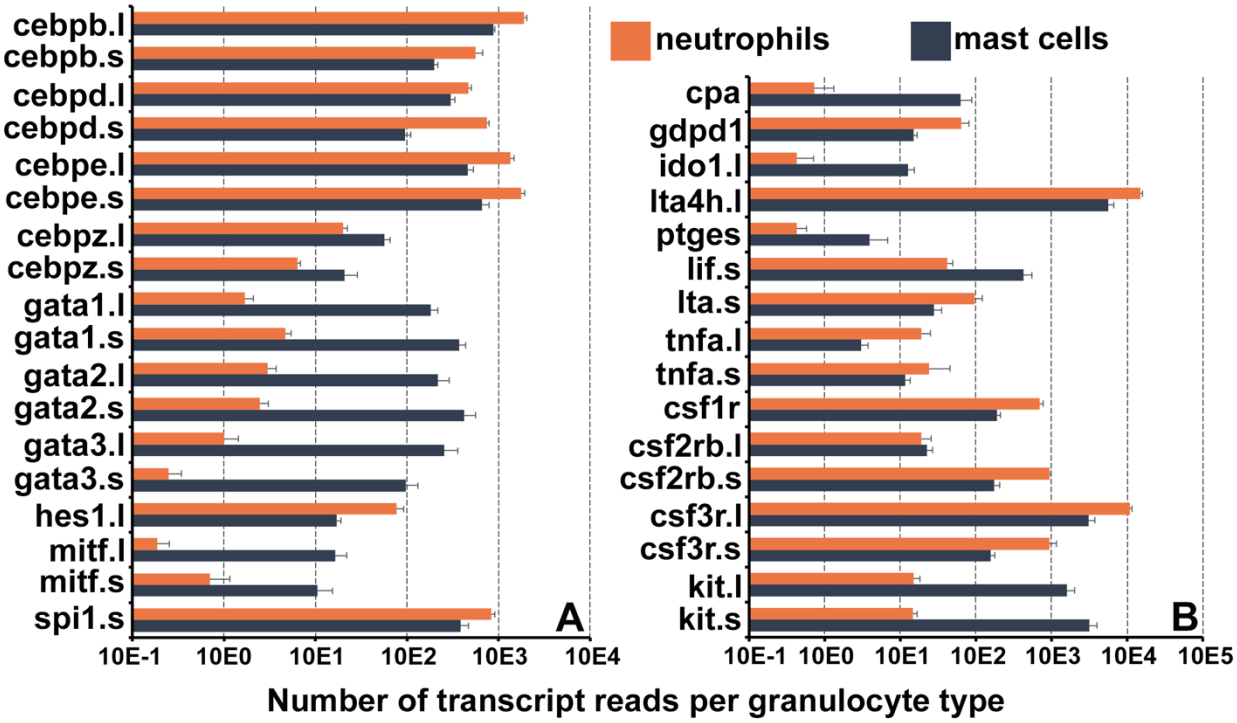

Figure 2. Frog mast cells and neutrophils possess gene profiles similar to their mammalian counterparts. The differentially expressed genes from the RNA sequencing analyses of *X. laevis* mast cells and neutrophil cultures were profiled for those encoding (**A**) transcription factors associated with mast cell- or neutrophil-specific lineages and (**B**) granulocyte antimicrobial components and growth factor receptor genes. All depicted genes were significantly differentially expressed between the two populations, *N*=4 per group.

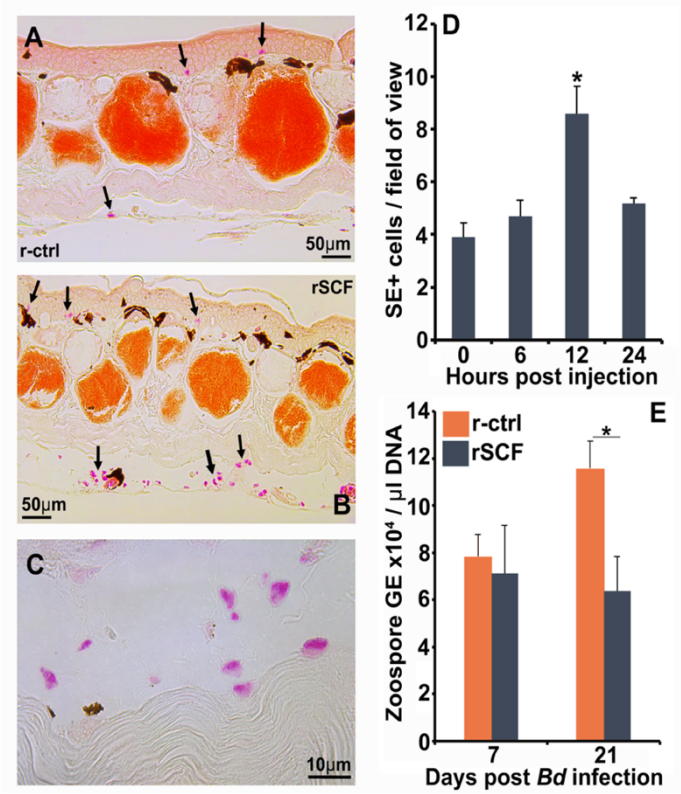

Figure. 3. Enriching frog cutaneous mast cells lowers *Bd* loads. Representative images of SE stained (**A**) control and (**B**) mast cell-enriched skin 12 hpi. (**C**) We confirmed the enriched population was composed of mono-morphonuclear cells. (**D**) Mast cell enrichment was optimized across several time points by quantifying SE-positive cells per field of view under 40x magnification. Results represent means ± SEM from 3 animals per time point (2 experimental repeats). (**E**) Mast cell-enriched and control dorsal skins were collected from *X. laevis* 7- and 21-dpi. *Bd* loads are represented as the number of zoospore genomic equivalents (GE) x 10^4 per µl of total input DNA. Time points were analyzed independently. Results represent means ± SEM from 7 animals per experimental group (N=7). Asterisks indicate significance: $p < 0.05$ by (**D**) one-way ANOVA with Tukey post-hoc analysis or (**E**) Student's t-test.

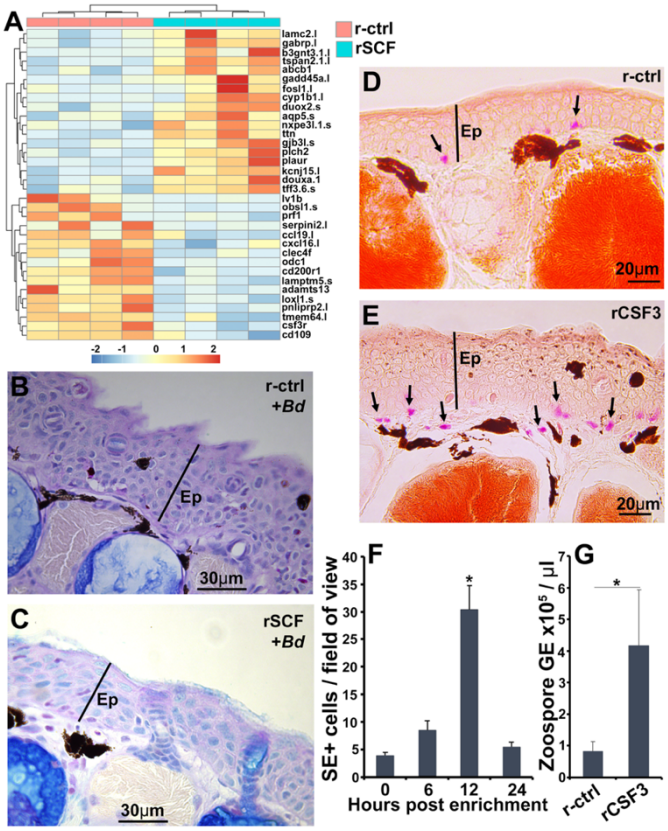

Figure. 4. Consequences of cutaneous mast cell and neutrophil enrichment. (**A**) RNAseq analysis of skin tissue from control (r-ctrl) or mast cell-enriched (rSCF) *Bd*-infected *X. laevis* at 21 dpi. Heat map of the top 30 DEGs, numbers matched to colors represent $\log^2$ fold change in expression. (**B** & **C**) Representative images of control and mast cell-enriched, *Bd*-infected skins, 21 dpi, demonstrating differences in epidermal thickening. (**D** & **E**) Representative images of control (r-ctrl) and neutrophil-enriched (rCSF3) skins collected 12 hpi demonstrating differences in epidermal thickening. (**F**) Kinetics of neutrophil enrichment following subcutaneous rCSF3 administration. Results are means $\pm$ SEM of SE-positive cells per field of view from 4 animals per time point (N=4). (**G**) *Bd* loads from control and neutrophil-enriched skin tissue 7 dpi, (N=6). Asterisks indicate significance: $p < 0.05$ by (**F**) one-way ANOVA with Tukey post-hoc analysis or (**G**) Student's t-test.

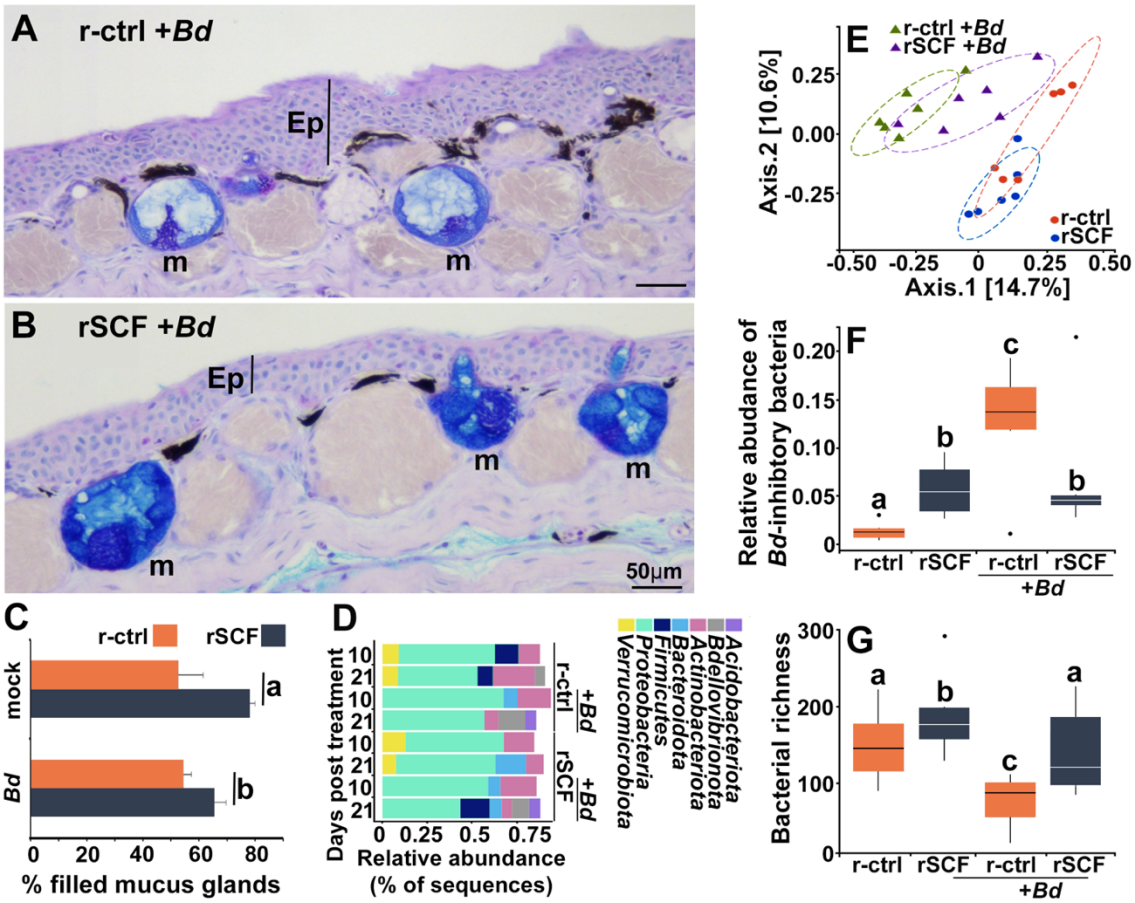

Figure. 5. Cutaneous mast cells promote filled mucus glands. Control (r-ctrl-injected) or mast cell-enriched (rSCF-injected) *X. laevis* were mock-infected or challenged with *Bd* for 21 days. Mucin content was examined in cutaneous mucus glands with Alcian Blue/PAS stain. Representative images of *Bd*-infected (**A**) control and (**B**) mast cell-enriched animals. Mucus glands are denoted by 'm', and epithelia are denoted by 'Ep'. (**C**) ImageJ software was used to determine the proportion of positive mucin staining within each mucus gland. Results are mean ± SEM percent positive mucin staining per mucus gland. Letters indicate group mean significance: $p < 0.05$ for treatment effects and interaction by two-way ANOVA. Skin tissue pieces from six individual frogs were used per treatment group (N=6). (**D**) Microbial phyla distribution across groups. Low abundance phyla (< 5% relative abundance are not shown). 10 dpi (**E**) community composition (Jaccard distances shown with 80% confidence ellipses) differed among all treatments. (**F**) Relative abundance of *Bd*-inhibitory bacteria and (**G**) bacterial richness were examined in control and mast cell enriched frogs, 10 days post *Bd* or mock challenge. Letters above bars in C, F and G indicate statistically different groups.

SUPPLEMENTARY MATERIALS

Production of recombinant cytokines: The *X. laevis* SCF and CSF3 sequences representing the signal peptide-cleaved transcripts were ligated into the pMIB/V5 His A insect expression vectors (Invitrogen). SCF-ligated, CSF3-ligated, or empty vectors were transfected into Sf9 insect cells (cellfectin II, Invitrogen). Recombinant proteins contain a V5 epitope, and western blot with an anti-V5-HRP antibody (Sigma) confirmed their presence. Positive transfectants were selected using 10 µg/mL blasticidin (Gibco). Expression cultures were scaled up to 500 mL liquid cultures, grown for 5 days, pelleted by centrifugation, and the supernatants collected. Supernatants were dialyzed overnight at 4°C against 150 mM sodium phosphate, concentrated against polyethylene glycol flakes (8 kDa) at 4°C, dialyzed overnight at 4°C against 150 mM sodium phosphate, and passed through Ni-NTA agarose columns (Qiagen). Columns were washed with 2 × 10 volumes of high stringency wash buffer (0.5% Tween 20, 50 mM Sodium Phosphate, 500 mM Sodium Chloride, 100 mM Imidazole) and 5 x 10 volumes of low stringency wash buffer (as above but with 40 mM Imidazole). Recombinant proteins were eluted with 250 mM imidazole. After recombinant protein purification, a halt protease inhibitor cocktail (containing AEBSF, aprotinin, bestatin, E-64, leupeptin and pepstatin A; Thermo Scientific) was added. Intact recombinant protein presence was confirmed again by western blot and the protein concentrations quantified by Bradford protein assays (BioRad). Protein aliquots were stored at -20°C until use.

Bone marrow granulocyte cultures: Bone marrow cells were isolated as previously described [58]. Briefly, adult *X. laevis* (approximately one year old) were euthanized in 5% tricaine mesylate followed by cervical dislocation. Femurs were removed and washed in ice-cold Amphibian-PBS (A-PBS) in sterile conditions. Each femur was flushed with 5 mL of A-PBS. Red blood cells were removed from culture via a differential gradient generated with 51% Percoll. Bone marrow cell counts were generated using trypan blue exclusion and cells were seeded at a density of 10^4 cells/well for gene expression experiments, $5x10^4$ cells/well for histology analyses, and 10^5 cells/well for electron microscopy analyses.

Histology: Paraffin-embedded tissue sections (5 µm) were deparaffinized, rehydrated through A-PBS, and stained with Naphthol AS-D Chloroacetate (specific esterase; Sigma) or Alcian Blue/PAS (Newcomer, Middleton, WI) according to the manufacturers' instructions and optimized

for *Xenopus* skin tissues. Cells collected from *in vitro* cultures were cytocentrifuged onto glass microscope slides (VWR). Cells were stained immediately with Giemsa (Sigma) for 7 minutes or fixed with 10% neutral buffered formalin for 30 minutes and stained with specific esterase according to the manufacturers' instructions. Slides stained with Alcian Blue/PAS (Newcomer) were used to quantify mucin content from *in vivo* experiments. Images were taken using identical microscope settings under 20x magnification. Images were converted to 8-bit in Fiji by ImageJ and threshold adjusted such that positive staining for mucus was captured within the mucus glands (threshold held constant across images). The percentage of each mucus gland positively stained and the average percent-positive per field of view were subsequently calculated. Positive staining of both acidic and neutral mucins was included in analyses. All slides were imaged with a Leica DMi8 Inverted Fluorescent Microscope with all mucus glands assessed for each respective frog skin section (Leica Microsystems, Davie, FL).

Analyses of immune gene expression and *Bd* skin loads: Cells and tissues were homogenized in Trizol reagent, flash frozen on dry ice, and stored at -80°C until RNA and DNA isolation. RNA isolation was performed using Trizol according to the manufacturer's directions. RNA-Seq is described in detail below. For qRT-PCR gene expression analysis, RNA (500 ng/sample) was reverse transcribed into cDNA using cDNA qscript supermix (Quantabio, Beverly, MA). Following RNA extraction, back extraction buffer (4 M guanidinethiocyanate, 50 mM sodium citrate, 1 M Tris pH 8.0) was mixed with the remaining Trizol layer and centrifuged to isolate the DNA-containing aqueous phase. DNA was precipitated overnight with isopropanol, pelleted by centrifugation, washed with 80% ethanol, and resuspended in TE buffer (10 mM Tris pH 8.0, 1 mM EDTA). DNA was purified by phenol:chloroform extraction and resuspended in molecular grade water (VWR).

Quantitative gene expression analyses for both *Bd* and *X. laevis* cells and tissues were performed using the CFX96 Real-Time System (Bio-Rad Laboratories, Hercules, CA) and iTaq Universal SYBR Green Supermix (Bio-Rad Laboratories). The Bio-Rad CFX Manager software (SDS) was employed for all expression analysis. All expression analyses were conducted using the ΔΔCt method relative to the *gapdh* endogenous control gene for *X. laevis.* Fungal load quantification was assessed by absolute qPCR. Isolated *Bd* DNA (JEL 197 isolate) was serially diluted and used as the standard curve. Primers were designed and validated against

the *Bd* ribosomal RNA internal transcribed spacer 1 (ITS1). The primers used are listed in Table S1.

Analyses of mucus *Bd*-killing capacities: Mucosomes were collected from mast cell- or vector-enriched *X. laevis* that were either mock- or *Bd*-infected for 10 or 21 days. To this end, individual *X. laevis* were soaked in a 5 mL water bath for 1 hour. Each water sample was then lyophilized, reconstituted with 500 µl of molecular grade water, and passed through a sterile cell strainer to remove large debris.

Bd was seeded in opaque white 96-well plates (20,000 zoospores in 50 µl of tryptone broth / well). Next, 50 µl of mucosome solution was added to each well (100 µl total well volume) in three replicate wells per individual *X. laevis* mucosome. Mucosomes, tryptone broth, and water were each plated alone as controls. Plates were sealed with parafilm and incubated at 19°C for 16 hrs with gentle mixing (20 rpm).

Zoospore viability was determined with the CellTiter-Glo 2.0 Cell Viability assay kit (Promega) according to the manufacturer's instructions and using a SpectraMax plate reader (Molecular Devices, San Jose, CA). Luminescence readings were fitted to a standard curve (descending proportions of heat-killed zoospores to viable zoospores) to calculate the number of viable zoospores in each well. Zoospores were heated-killed at 65°C for 15 mins.

Skin microbiome analyses: All analyses were performed in the R environment version 4.0.3 (R Core Team, 2020). Demultiplexed reads were imported from Basespace into R environment for sequence processing. Package "dada2"[61] was used to perform quality filtering using their standard filtering parameters (*i.e.*, maxEE = 2), which collapsed high quality reads into amplicon sequence variant (ASV) and removed chimeras. Bacterial taxonomy was assigned using Silva version 138.1. The R package "phyloseq"[62] was used to import and merge the final ASV table, taxonomy table, and metadata to create a phyloseq object to perform further analyses. Sequences classified as cyanobacteria/chloroplast and those unclassified at kingdom were removed. Singletons were filtered out (*i.e.*, ASVs with only one sequence read in one individual). The R package "decontam"[63] was used to remove potential contaminants using the method "combined." The ZymoBIOMICS microbial community standards (positive controls) were analyzed, and we found genera in similar relative abundances as described by Zymo.

To determine how *Bd* and mast cell treatments impacted skin microbiomes, the microbiome structure was examined. The components of microbiome structure were: ASV richness (measured as *Bd*-inhibitory ASV richness and total ASV richness), microbial composition (measured by Jaccard and Bray-Curtis distances), and sequence abundance of *Bd*-inhibitory ASVs (measured as individual *Bd*-inhibitory ASV sequence counts and total relative abundance of *Bd*-inhibitory ASVs). To characterize variation in microbiome structure, Mast Cell (mast cell normal and mast cell+), *Bd* (*Bd*- and *Bd*+) and their interaction as explanatory variables at two-time points Day 10 and Day 21 post *Bd* infection were included. For this characterization, log-transformed ASV richness in ANOVAs, microbial composition measures in PERMANOVAs and log-transformed raw sequence counts in ANOVAs (with post-hoc corrections for multiple comparisons) were used. For identification of *Bd*-inhibitory ASVs, methods as described in by Jimenez *et al*., 2022[64] were followed.

Table S1. List of primer sequences

Target Name	Primer Sequence (5'→ 3')
***Bd* its1 sense**	GCCATATGTCACGAGTCGAA
***Bd* its1 antisense**	GCCAAGAGATCCGTTGTCA
gapdh sense	GACACTCACTCCTCCATCTTTG
gapdh antisense	TGCTGTAGCCGCATTCATTA
hdc sense	GAATCTGAAAGCTGGGAGAGAA
hdc antisense	GATGTCAGGGCAGGAAAGTAG
il4 sense	GACATCAAGGACACCTGAAGAA
il4 antisense	GTCACAGGGAATCGGTACTAAAC
mag sense	GGCCTTTGCAGATGAAGATTTAG
mag antisense	CTACTGCTTCTGCATCTCGTT
pgla sense	CTGCACTCTGTGCAACCATAA
pgla antisense	CTCCAGCTTTAGATGCCATTCC

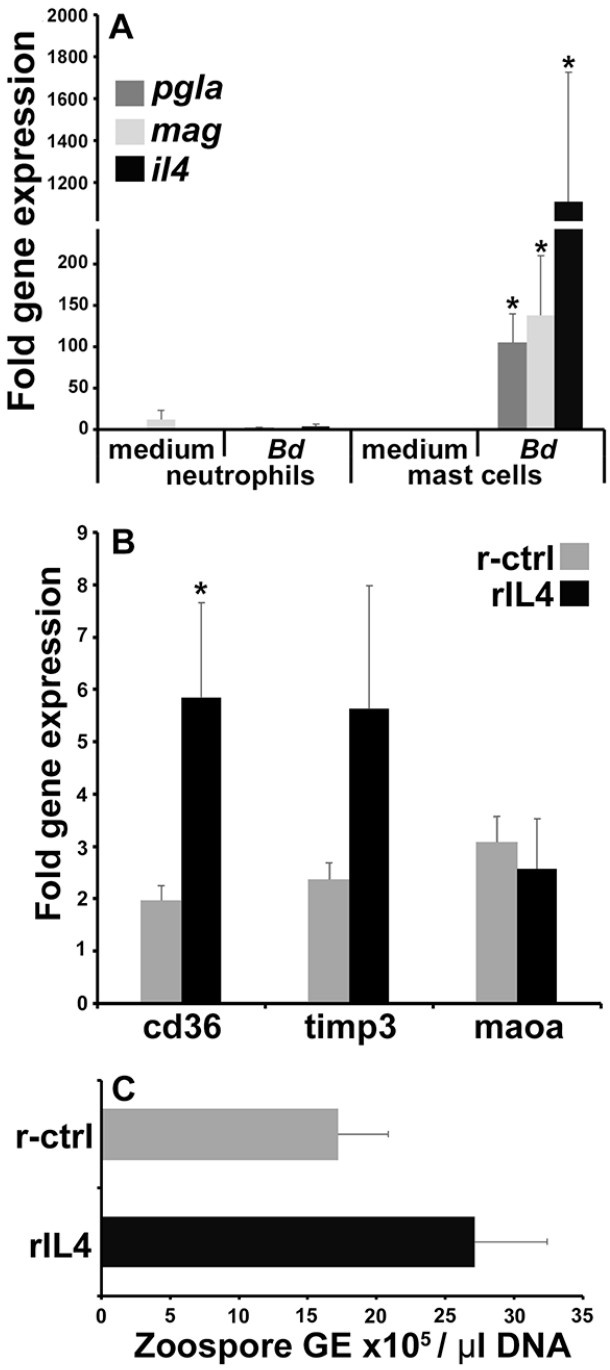

Figure. S1. *In vitro* analyses of frog mast cells and neutrophils challenged with *Bd* (**A**) Mast cells and neutrophils derived from bone marrow of 6 individual frogs (*N*=6) were co-cultured with *Bd* (5 fungal cells per granulocyte) for 6 hrs prior to gene expression analyses of the antimicrobial peptide genes PGLa (*pgla*) and magainin (*mag*) or interleukin-4 (*il4*). (**B**) Changes in gene expression of selected genes in skin following subcutaneous injection of rIL4 (*N*=7). (**C**) Frogs were exposed to *Bd* and 24 hrs later injected subcutaneously with rIL4 or r-ctrl. Skin *Bd* loads were assessed 9 days following injection (*N*=8, per group). For B, asterisks denote statistically significant differences in expression following *Bd*-challenge compared to medium controls in mast cell cultures, one-way ANOVA with Tukey post-hoc analysis $p < 0.05$. For C, asterisk indicates significantly increased expression of cd36 by Student's t test, $p < 0.05$.

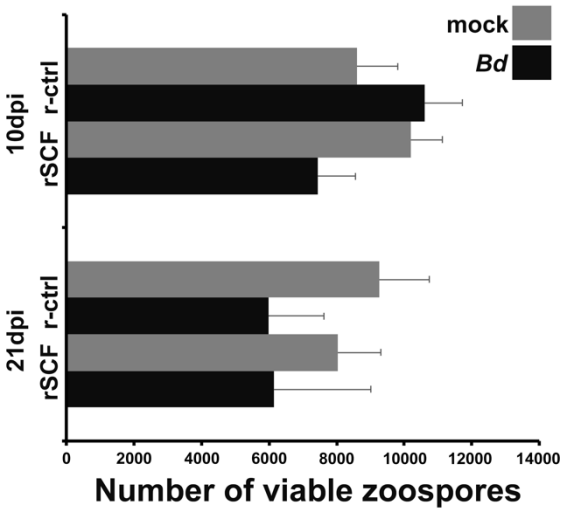

Figure. S2. Mucosomes from mast cell-enriched frogs do not confer *Bd* killing. Differences in musocome-killing capacities were determined by incubating zoospores with total mucosome contents for 16 hrs. Mucosomes were acquired from 10- or 21-day mock- or *Bd*-infected *X. laevis* that were injected with rSCF (mast cell-enriched) or r-ctrl (control). Results are mean $\pm$ SEM and were analyzed via a two-way ANOVA; 10- and 21-day experimental groups were analyzed independently; alpha set at 0.05. N = 5 experimental animals per treatment group for 10 dpi analyses and N= 8 experimental animals per treatment group for 21 dpi analyses.

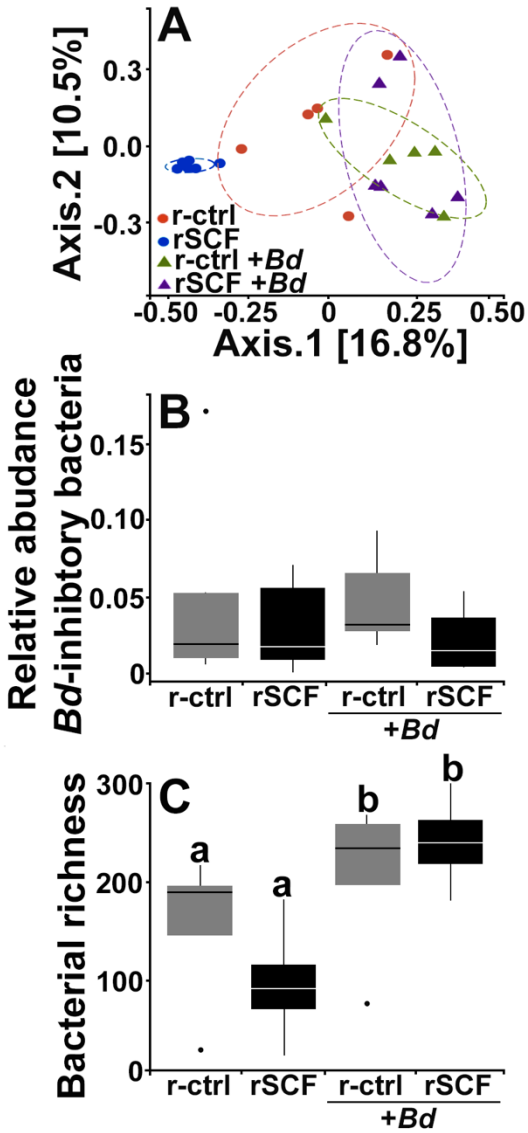

Figure. S3. Mast cell enrichment protects frogs from *Bd*-mediated changes to skin microbiomes. 21 days post mock or *Bd*-challenge, we examined (**A**) community composition (Jaccard distances shown with 80% confidence ellipses), (**F**) relative abundance of *Bd*-inhibitory bacteria and (**G**) bacterial richness. Letters above bars indicate statistically distinct groups.